Soliton generation in optical fibers for a dual-frequency input

N.-C. Panoiu
Department of Physics, New York University, 4 Washington Place, New York, New York 10003
and Department of Theoretical Physics, Institute of Atomic Physics, P.O. Box MG-6, Bucharest, Romania

I. V. Mel'nikov
General Physics Institute of the Russian Academy of Sciences, ul. Vavilova 38, Moscow 117942, Russian Federation

D. Mihalache
Department of Theoretical Physics, Institute of Atomic Physics, P.O. Box MG-6, Bucharest, Romania

C. Etrich and F. Lederer
Institute of Solid State Theory and Theoretical Optics, Friedrich Schiller University Jena, Max-Wien-Platz 1, Jena, D-07743, Germany
(Received 26 April 1999)

We analyze scenarios of soliton generation in an ideal fiber for an input that consists of either two in-phase or out-of-phase solitonlike optical pulses at different frequencies. In both cases the relationship between the structure of the emerging solitons and the frequency separation of the initial solitons is studied both analytically and numerically. Depending on the value of the frequency detuning, if the two initial solitons are in phase (symmetric input), two bound solitons with equal amplitudes (breather), a single soliton, or a pair of solitons, which have equal amplitudes and exhibit opposite velocities, can be generated. When the two initial solitons are out-of-phase (antisymmetric input), only the last scenario takes place. Also, we calculated the threshold values of the frequency separation at which the structure of the emerging solitons changes. Moreover, we demonstrated that two of these critical frequencies correspond to cusplike maxima of the energy density of the radiative modes. Finally, we show that these analytical results are entirely verified by numerical simulations. [S1063-651X(99)01910-8]

PACS number(s): 42.65.Tg, 42.81.Dp, 02.30.Jr

I. INTRODUCTION

The idea of using optical solitons as carriers of information in high-speed communication systems was first proposed in the seminal papers of Hasegawa and Tappert [1]. By taking into account the intrinsic Kerr nonlinearity of silica, they showed that the propagation of optical pulses in both the anomalous dispersion regime (negative group velocity) and the normal dispersion regime (positive group velocity) is governed by similar types of nonlinear Schrödinger equations (NLSE). As it is well known, both of these equations are completely integrable and their solutions can be found by the inverse scattering transform (IST) [2]. One of the most important characteristics of an equation solvable by the IST is that it possesses solutions which propagate without any distortion of their shape, the so-called soliton solutions. In the case of the NLSE, the mechanism by which these solitons are formed is well understood: they can be viewed as the outcome of the balanced interplay between the group-velocity dispersion and the nonlinearly induced self-phase modulation. More exactly, the robustness of the soliton solutions stems from the fact that their wave numbers are separated from those of linear dispersive waves so that there is no resonant exchange of energy between the nonlinear and linear modes.

In the early 1980s, as the fiber optics technology advanced, the experimental verification of the propagation of optical solitons was possible. Thus, in a series of elegant experiments, it was demonstrated that in the region of anomalous dispersion it is possible to propagate *bright* solitons [3] while in the region of normal dispersion *dark* solitons can be excited [4].

As it is well known, the equation governing the nonlinear pulse evolution in an ideal optical fiber in the anomalous dispersion regime is the following NLSE:

$$i\frac{\partial\psi}{\partial t}+\frac{\partial^2\psi}{\partial x^2}+2|\psi|^2\psi=0. \tag{1}$$

Here we adopt the notations in the mathematical literature, that is, the variable t plays the role of the evolution variable. However, we stress that the physical meaning of the variable t is the normalized distance along the fiber, x represents the normalized time, and ψ is the normalized complex amplitude of the pulse envelope. The normalized units are $t=|\beta_2|Z/2T_0^2$ and $x=(T-Z/v_g)/T_0$, where β_2 is the group-velocity dispersion coefficient, T_0 is the pulse width ($T_{\mathrm{FWHM}}=1.763T_0$), v_g is the group velocity, and Z and T are the physical distance and time, respectively (FWHM denotes full width at half maximum).

In spite of the fact that a single optical soliton can propagate over very long distances without experiencing any deformation of its shape, in order to be used as bits of information in reliable high-speed communication systems one has to create stable propagating trains of well separated solitons. Therefore, it is important to understand the interaction between adjacent solitons belonging to such a train. This interaction has mainly two components. The first one is de-

termined by the nonlinear interaction among solitons when all other perturbations are neglected. To be more specific, we stress that the linear superposition of N solitons does not lead to an N-soliton state whose parameters are described simply by a linear combination of the parameters of the initial solitons. Instead, there is a very intricate (nonlinear) relationship between the parameters which describe the emerging N-soliton state and the parameters of the N initial solitons. The effects of the nonlinear interaction between copropagating solitons in the absence of any perturbative factors have been thoroughly investigated both analytically [5–9] and numerically [5,10]. The second component of the nonlinear interaction among solitons in a soliton train is given by the influence of various perturbative factors on the parameters of the propagating solitons. In order to describe this interaction, usually one assumes that the parameters of the solitons slowly change upon the action of perturbations and so one is able to determine their dependence on the propagation distance along the optical fiber. This was performed in [11–19] for $N=2$ solitons and in [9,10,20] for $N\geqslant 3$ solitons.

In order to increase the transmission capacity (bit rate) of soliton-based communication systems, channels at different wavelengths can be used. However, solitons in different channels interact because of the cross-phase modulation and this can have a deleterious influence on the bit rate of the transmission line. Therefore, one needs to understand the interaction between overlapped solitons of different frequencies. This problem has been addressed only in its limit cases, when the frequency detuning is much smaller [19] or much larger [7,8,21–24] than the spectral width of the solitons. In the first case the interacting solitons propagate in the same channel while in the later case they propagate in different channels.

In this paper we analyze the nonlinear interaction between two superimposed solitons with different frequencies when the frequency detuning is comparable with the soliton frequency width. We discuss the structure of the emerging solitons without taking into account any interaction with external perturbative factors. The paper is organized as follows. In Sec. II we give a brief summary of the IST and soliton solutions of Eq. (1). Then, in Sec. III we present the structure of the emerging solitons from a linear superposition of two in-phase solitons with different frequencies (symmetric input). In Sec. IV, by a similar analysis to that in Sec. III, we present the structure of the optical field in the case in which the two solitons are out-of-phase (antisymmetric input). Furthermore, the critical values of the detuning frequencies at which the structure of the emerging solitons changes are calculated in Sec. V. Moreover, the results established in this section are used to describe the structure of the emerging optical field which corresponds to the case in which there is an arbitrary phase difference between the two overlapping solitons. Finally, in the final section, the results are summarized and discussed.

II. INVERSE SCATTERING TRANSFORM

In this section we briefly review the IST method, focusing on its application to the NLSE. This method consists mainly in the following three steps. First, by using the initial condition $\psi(x,0)$, a spectral problem associated with the NLSE is solved and so the initial scattering data are determined (direct scattering analysis). These data contain the spectrum of a linear differential operator: the discrete part of the spectrum determines the properties of the soliton component of the solution while the continuous part describes the radiation field. In the second step, by using the time evolution of the scattering data, their values at an arbitrary time t are obtained. This step is rather trivial as the discrete part of the spectrum does not change in time while the continuous part satisfies a simple linear differential equation. Finally, in the last step, the solution $\psi(x,t)$ is reconstructed from the scattering data at the time t (the inverse scattering transform). In what follows, we will describe the steps outlined above. To begin with, let us consider the following two systems of equations:

$$\frac{\partial F}{\partial x}=UF, \tag{2}$$

$$\frac{\partial F}{\partial t}=VF, \tag{3}$$

where U and V are 2×2 matrices given by the following formulas:

$$U=\begin{pmatrix} \frac{\lambda}{2i} & i\bar{\psi} \\ i\psi & -\frac{\lambda}{2i} \end{pmatrix}, \tag{4}$$

$$V=\begin{pmatrix} -\frac{\lambda^2}{2i}-i|\psi|^2 & -i\lambda\bar{\psi}+\frac{\partial\bar{\psi}}{\partial x} \\ -i\lambda\psi-\frac{\partial\psi}{\partial x} & \frac{\lambda^2}{2i}+i|\psi|^2 \end{pmatrix}. \tag{5}$$

F is a vector-valued function, λ is a spectral parameter, and the overbar signifies complex conjugation. In the above formulas, as well as in the subsequent presentation, we use the notations in [25]. With this choice of the matrices U and V, it is easy to verify that the compatibility condition for the systems (2) and (3), the so-called *zero curvature representation*,

$$\frac{\partial U}{\partial t}-\frac{\partial V}{\partial x}+[U,V]=0, \tag{6}$$

is equivalent to the NLSE (1). Next, for real values λ we introduce the Jost functions $T_{\pm}(x;\lambda)$ associated with the eigenvalue problem (2). These are 2×2 matrices whose columns are the two linearly independent solutions of Eq. (2). They have the following asymptotic behavior:

$$T_{\pm}(x;\lambda)\rightarrow E(x;\lambda), x\rightarrow\pm\infty, \tag{7}$$

where $E(x;\lambda)\equiv\exp((\lambda x/2i)\sigma_3)$, with σ_i $(i=1,2,3)$ the standard 2×2 Pauli matrices. Because the columns of the matrix $T_{-}(x;\lambda)$ are linearly dependent on the columns of the matrix $T_{+}(x;\lambda)$, one can write

$$T_{-}(x;\lambda)=T_{+}(x;\lambda)T(\lambda), \tag{8}$$

where $T(\lambda)$ is the scattering matrix. It is easy to see that the matrix $U(x;\lambda)$ has the symmetry property $\overline{U}(x;\lambda) = \sigma_2 U(x,\overline{\lambda})\sigma_2$ and, obviously, for real λ this symmetry relation extends to the scattering matrix: $\overline{T}(\lambda) = \sigma_2 T(\lambda)\sigma_2$. This leads to the general expression for the matrix $T(\lambda)$:

$$T(\lambda) = \begin{pmatrix} a(\lambda) & -\overline{b}(\lambda) \\ b(\lambda) & \overline{a}(\lambda) \end{pmatrix}, \tag{9}$$

where $a(\lambda)$ and $b(\lambda)$ are the scattering (Jost) coefficients and are given by

$$a(\lambda) = \det(T_-^{(1)}(x;\lambda), T_+^{(2)}(x;\lambda)), \tag{10}$$

$$b(\lambda) = \det(T_+^{(1)}(x;\lambda), T_-^{(1)}(x;\lambda)). \tag{11}$$

Here, the first and the second columns of the Jost functions were denoted by $T_\pm^{(1)}(x;\lambda)$ and $T_\pm^{(2)}(x;\lambda)$, respectively. One can prove that, if the initial condition $\psi(x,0)$ decreases asymptotically to zero when $|x|\to\infty$ faster than any power of x, then $T_-^{(1)}(x;\lambda)$, $T_+^{(2)}(x;\lambda)$, and, consequently, the scattering coefficient $a(\lambda)$ can be analytically extended in the upper half of the λ-complex plane while $T_-^{(2)}(x;\lambda)$ and $T_+^{(1)}(x;\lambda)$ can be analytically extended in the lower half of the λ-complex plane.

The soliton solutions of Eq. (1) are determined by the set of zeros of $a(\lambda)$: $\mathcal{Z} = \{\lambda_i \in \mathbf{C} | a(\lambda_i) = 0,\ \mathrm{Im}(\lambda_i) > 0,\ i = 1, \ldots, n\}$. As Eq. (10) shows, if $\lambda = \lambda_i$ is a zero of $a(\lambda)$, the column $T_-^{(1)}(x;\lambda_i)$ is proportional to the column $T_+^{(2)}(x;\lambda_i)$ so that, if one denotes by γ_i the proportionality coefficient, one can write

$$T_-^{(1)}(x;\lambda_i) = \gamma_i T_+^{(2)}(x;\lambda_i). \tag{12}$$

The zeros of $a(\lambda)$, together with the complex coefficients γ_i, $i = 1, \ldots, n$, completely define the soliton part of the solution of Eq. (1) while the Jost coefficients $a(\lambda)$ and $b(\lambda)$ with λ on the real axis describe the radiative part.

The general solution of Eq. (1) can be obtained by solving the Gelfand-Levitan-Marchenko (GLM) equation

$$\Gamma_+(x,y) + \Omega(x+y) + \int_x^\infty \Gamma_+(x,s)\Omega(s+y)ds = 0, \tag{13}$$

where the kernel $\Gamma_+(x,y)$ is a 2×2 matrix defined by the following integral representation of the Jost functions $T_+(x;\lambda)$:

$$T_+(x;\lambda) = E(x;\lambda) + \int_x^\infty \Gamma_+(x,y)E(y;\lambda)dy \tag{14}$$

and the 2×2 matrix $\Omega(x)$ is determined by the spectrum of the linear differential operator appearing in Eq. (2):

$$\Omega(x) = \omega(x)\sigma_- - \overline{\omega}(x)\sigma_+ \tag{15}$$

with

$$\omega(x) = \frac{1}{4\pi}\int_{-\infty}^{\infty} \frac{b(\lambda)}{a(\lambda)} e^{i\lambda x/2} d\lambda + \frac{1}{2i}\sum_{j=1}^{n} c_j e^{i\lambda_j x/2}. \tag{16}$$

Here, $c_j = \gamma_j / \dot{a}(\lambda_j)$ and the dot represents the derivative with respect to λ. Once the kernel $\Gamma_+(x,y)$ is determined from the GLM equations, the general solution of Eq. (1) can be found from the following relation:

$$\sigma_3 U_0(x) = [\Gamma_+(x,x), \sigma_3], \tag{17}$$

where $U_0(x) = i(\overline{\psi}\sigma_+ + \psi\sigma_-)$. So, once the scattering data $a(\lambda), b(\lambda), \lambda_i, \gamma_i$, $i = 1, \ldots, n$ are known, by using Eqs. (13) and (17) one can find the general solution of Eq. (1). However, we mention that the solution of the GLM equation (13) can be found in a closed form only if the scattering coefficient $b(\lambda) = 0$ for λ on the real axis.

Similar to the matrices $U(x;\lambda)$ and $T(\lambda)$, the kernel $\Gamma_+(x,y)$ has the symmetry property $\overline{\Gamma}_+(x,y) = \sigma_2\Gamma_+(x,y)\sigma_2$. Therefore, it can be written as

$$\Gamma_+ = \begin{pmatrix} \Gamma_+^{11} & -\overline{\Gamma}_+^{12} \\ \Gamma_+^{12} & \overline{\Gamma}_+^{11} \end{pmatrix}. \tag{18}$$

Next we discuss the time evolution of the scattering data. This dynamics can be obtained from Eq. (3) and the fact that the function $\psi(x,0)\to 0$ for $|x|\to\infty$. Without any proof, we present here only the results. Thus, one can show that the spectral parameter λ and the scattering coefficient $a(\lambda)$ do not change upon propagation while the scattering coefficient $b(\lambda)$ and the complex coefficients γ_i, $i = 1, \ldots, n$ have the following time dependence:

$$b(\lambda,t) = b(\lambda,0)e^{-i\lambda^2 t}, \tag{19}$$

$$\gamma_j(t) = \gamma_j(0)e^{-i\lambda_j^2 t}. \tag{20}$$

To conclude this section, we introduce the integrals of motion of the NLSE. As it is known, this equation has an infinite number of integrals of motion which are in involution with respect to a certain Poisson structure. From a physical point of view, the most useful are the number of particle N, the momentum P, and the Hamiltonian H. They are given by the following expressions:

$$N = \int_{-\infty}^{\infty} |\psi|^2 dx = 2\sum_{i=1}^{n} \eta_i - \frac{1}{\pi}\int_{-\infty}^{\infty} \ln|a(\lambda)| d\lambda, \tag{21}$$

$$P = \frac{1}{2i}\int_{-\infty}^{\infty} \left(\frac{\partial\psi}{\partial x}\overline{\psi} - \frac{\partial\overline{\psi}}{\partial x}\psi \right) dx$$

$$= 2\sum_{i=1}^{n} \eta_i\xi_i - \frac{1}{\pi}\int_{-\infty}^{\infty} \lambda \ln|a(\lambda)| d\lambda, \tag{22}$$

$$H = \int_{-\infty}^{\infty} \left(\left|\frac{\partial\psi}{\partial x}\right|^2 - |\psi|^4 \right) dx$$

$$= 2\sum_{i=1}^{n} \left(\eta_i\xi_i^2 - \frac{1}{3}\eta_i^3 \right) - \frac{1}{\pi}\int_{-\infty}^{\infty} \lambda^2 \ln|a(\lambda)| d\lambda, \tag{23}$$

where $\eta_i = \mathrm{Im}\,\lambda_i$ and $\xi_i = \mathrm{Re}\,\lambda_i$.

III. SOLITON GENERATION FROM SYMMETRIC INPUT PULSES

In this section we analyze the structure of the optical field generated from a linear symmetric superposition of two fundamental solitons with different frequencies. Such an initial condition of Eq. (1) can be written as

$$\psi(x,0) = \mathrm{sech}(x)e^{i\omega x} + \mathrm{sech}(x)e^{-i\omega x}, \tag{24}$$

where 2ω is the frequency detuning between the two solitons. The symmetry implied by the initial condition (24), that is, $\psi(x,0) = \psi(-x,0)$, extends to the matrix $U(x;\lambda)$, so that it has the additional involution property

$$U(x;\lambda) = -\sigma_1 \overline{U}(-x;-\overline{\lambda})\sigma_1. \tag{25}$$

By taking into account the structure of the linear eigenvalue problem (2), it is easy to see that the symmetry (25) implies that if $F(x;\lambda)$ is an eigenfunction of Eq. (2) corresponding to the eigenvalue λ, then $\sigma_1\overline{F}(-x;\lambda)$ is an eigenfunction corresponding to the eigenvalue $-\overline{\lambda}$. Therefore, the discrete eigenvalues of the linear problem (2) are located symmetrically with respect to the imaginary axis. Furthermore, by taking into account the asymptotic behavior (7) of the Jost functions, one obtains that the eigenfunctions of Eq. (2) corresponding to the eigenvalues λ and $-\overline{\lambda}$ are related by the following relationship:

$$T_-^{(1)}(x;\lambda) = \sigma_1 \overline{T_+^{(2)}}(-x;-\overline{\lambda}), \tag{26}$$

$$T_-^{(2)}(x;-\lambda) = \sigma_1 \overline{T_+^{(1)}}(-x;\overline{\lambda}). \tag{27}$$

Here it was supposed that $\mathrm{Im}\,\lambda > 0$, that is, it belongs to the domain of analyticity of $T_-^{(1)}$ and $T_+^{(2)}$. The above equations, together with Eqs. (10) and (11), lead to the conclusion that the scattering coefficients must have the following symmetry property:

$$a(\lambda) = \overline{a}(-\overline{\lambda}) \tag{28}$$

for $\mathrm{Im}\,\lambda \geq 0$, and

$$b(\lambda) = -\overline{b}(-\lambda) \tag{29}$$

for real λ. This implies that the zeros of the scattering coefficient $a(\lambda)$ are located either on the imaginary axis or they appear in pairs at $(\lambda, -\overline{\lambda})$. Here we mention that a similar situation was encountered in the case of a perturbed NLSE [26,27]. However, in that case the zeros of the scattering coefficients appear in pairs for any arbitrary initial condition and not only for those with a specific symmetry. Moreover, it was proven in [28] that the structure of a soliton solution of that perturbed NLSE which corresponds to a pair of zeros is preserved even if the solitons propagate under the action of a general perturbation. In the present case this is no longer true: only perturbations which have the same symmetry as the initial condition (24) will preserve the structure of the zeros of the scattering coefficient $a(\lambda)$.

Now let us describe the case in which the only zeros of the coefficient $a(\lambda)$ are located at $(\lambda_0, -\overline{\lambda_0})$ with $\lambda_0 = \xi + i\eta$, ξ, $\eta > 0$, and $b(\lambda) = 0$ for any real λ. If we denote by (γ_+, γ_-) the proportionality coefficients defined by Eq. (12), one can see that Eq. (26) implies that

$$\overline{\gamma}_+ \gamma_- = 1. \tag{30}$$

Moreover, if we take into account the time dependence (20) of these coefficients, we see that this relation is satisfied at any time t, that is, the soliton solution preserves its initial symmetry. Furthermore, one can see from Eqs. (13) and (16) that if we choose the initial values of γ's such that

$$\gamma_+(0) = \gamma_-(0) = i, \tag{31}$$

then the initial condition $\psi(x,0)$ corresponding to these scattering data is real. This proves that, contrary to one of the results in [5], real symmetric pulses can generate pairs of solitons with nonzero velocity.

By solving the GLM equation (13) which corresponds to a pair of zeros located symmetrically with respect to the imaginary axis and with coefficients γ_+, γ_- which satisfy Eq. (31), one obtains the following two-soliton solution:

$$\psi(x,t) = \xi\eta e^{\phi(t)} \frac{e^{i\xi x}\cosh[\eta(x+2\xi t) + i\varphi] + e^{-i\xi x}\cosh[\eta(x-2\xi t) - i\varphi]}{\xi^2 \cosh\eta(x+2\xi t)\cosh\eta(x-2\xi t) + \eta^2 \sin\xi(x+2i\eta t)\sin\xi(x-2i\eta t)}, \tag{32}$$

where the overall phase $\phi(t) = -i(\xi^2 - \eta^2)t + \alpha$, $\alpha = \ln|\lambda_0|$, and $\tan\varphi = \eta/\xi$. This function corresponds to a pair of solitons with equal amplitudes η and with equal and opposite velocities ξ. As mentioned before, it preserves the initial symmetry during the propagation, that is, $\psi(x,t) = \psi(-x,t)$, and is real at $t = 0$.

In order to verify these results, we considered as the initial condition for the NLSE (1) the real, symmetric superposition (24) of two fundamental solitons. Thus, by using a numerical algorithm based on the IST [29], we determined the spectrum of the linear eigenvalue problem (2) which corresponds to the initial condition (24). In order to do this, we discretized the interval $(-L, L)$ into $2M+1$ subintervals of equal sizes. Within each such subinterval the function $\psi(x,0)$ was taken to be constant, while for $|x| \geq L$ we chose $\psi(x,0) = 0$. Then, in order to advance the eigenfunctions one step, we solved Eq. (2) by using a standard exponential propagator method. Thus, by knowing a solution of Eq. (2) at $x = -L$, by successive iterations one can find it at $x = L$. Furthermore, by choosing as the initial value of the solution at $x = -L$ the one given by Eq. (7), one can relate the Jost functions at $x = -L$ and $x = L$. This information allows us to

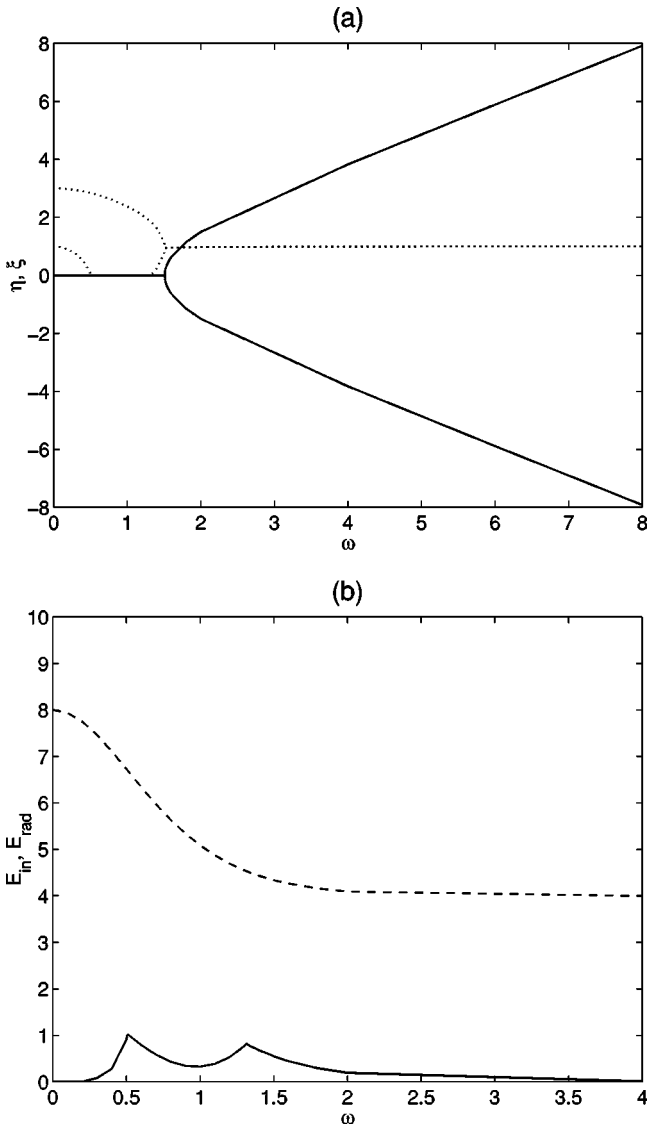

FIG. 1. The discrete spectrum determined by the symmetric input (24) and the energies in the optical field at the output. (a) The amplitude η (dotted line) and the velocity ξ (continuous line) of the generated solitons as a function of the frequency detuning ω; (b) the energies $E_{\rm in}$ (dashed line) and $E_{\rm rad}$ (continuous line) versus ω.

determine the scattering matrix and, implicitly, the scattering coefficients $a(\lambda)$ and $b(\lambda)$. In order to compute the zeros of the scattering coefficient $a(\lambda)$, we used a standard Newton-Raphson method. The numerical values of the parameters L and M were increased gradually until the computed values of the scattering data converged to an asymptotic value. Then, by using these scattering data, we calculated the energy carried by the emerging solitons as well as the amount of energy carried by the radiative modes. In Fig. 1(a), the spectrum of the linear eigenvalue problem (2) for the symmetric initial condition (24) is presented. As one can see, as the frequency detuning ω varies, three different kinds of solitons can be generated. First, for $\omega<\omega_1^s\simeq 0.505$ the coefficient $a(\lambda)$ has two distinct zeros located on the imaginary axis, so that a bound state consisting of two solitons with zero velocities (breather) emerges. Furthermore, for $\omega_1^s<\omega<\omega_2^s\simeq 1.313$ the coefficient $a(\lambda)$ has only one zero located on the imaginary axis so that for frequencies ω in this domain only a single soliton with zero velocity can be generated. If the frequency ω is further increased, $\omega_2^s<\omega<\omega_3^s\simeq 1.509$, again the coefficient $a(\lambda)$ has two zeros on the imaginary axis so that again a breather emerges. Finally, if $\omega_3^s<\omega$, the coefficient $a(\lambda)$ has two zeros situated symmetrically with respect to the imaginary axis so that the emerging solution is the two-soliton solution (32). As a final remark related to the discrete spectrum in the symmetric case, we mention that, as Fig. 1(a) illustrates, for frequencies $\omega\gg 1$ the velocity of the emerging solitons is $\xi\simeq\omega$. This result can be understood by noting that for large values of ω, the nonlinear interaction between the two superimposed solitons is very weak so that we expect that the amplitude and velocity of the initial solitons are only slightly perturbed by their interaction. More exactly, if $\omega\gg 1$, the frequency shift $|\xi-\omega|$ is inversely proportional to the square of the soliton width and the frequency detuning ω [7,8,21].

Furthermore, by using the expression of the input pulse and the scattering data, we calculated the total energy $E_{\rm in}$ of the initial pulse, the energy of the emerging solitons $E_{\rm sol}$, and the energy in the radiative modes $E_{\rm rad}$. Obviously, they must satisfy the relation $E_{\rm in}=E_{\rm sol}+E_{\rm rad}$. These energies are defined by the following relations:

$$E_{\rm in}=\int_{-\infty}^{\infty}|\psi(x,0)|^2dx, \tag{33}$$

$$E_{\rm sol}=2\sum_{i=1}^{n}\eta_i, \tag{34}$$

$$E_{\rm rad}=-\frac{1}{\pi}\int_{-\infty}^{\infty}\ln|a(\lambda)|d\lambda, \tag{35}$$

and do not change upon propagation. As was pointed out in Sec. II, in the IST theory the above quantities have the meaning of the number of particles, but here we use their physical interpretation, that is, the energy of the optical field. The dependence on ω of the total energy $E_{\rm in}$ and the energy in the radiative modes $E_{\rm rad}$ is presented in Fig. 1(b). One important fact that this figure illustrates is that the energy of the radiative modes $E_{\rm rad}(\omega)$ has two peaks at the threshold frequencies ω_1^s,ω_2^s. Consequently, the generated solitons will be influenced by the radiative field especially when the frequency detuning ω is close to these two threshold values. The origin of these two peaks can be understood if we take into account the spectrum shown in Fig. 1(a). Thus, for $\omega=\omega_{1,2}^s$ the scattering coefficient $a(\lambda)$ has one zero on the real axis, that is, $a(0)=0$. Therefore, the integrand in Eq. (35) has a logarithmic singularity at these two critical values of the frequency detuning ω.

As a further check of the results presented above, we determined numerically the solution of the NLSE (1) corresponding to the initial condition (24), and the results for some specific values of the frequency detuning ω are presented in Figs. 2(a)–2(d). As one can see, at $\omega=0.1$ and $\omega=1.4$ a breather emerges, at $\omega=1.0$ one obtains only one soliton with zero velocity, while for $\omega=1.525$ the emerging solution represents a two-soliton solution with equal amplitudes and opposite velocities.

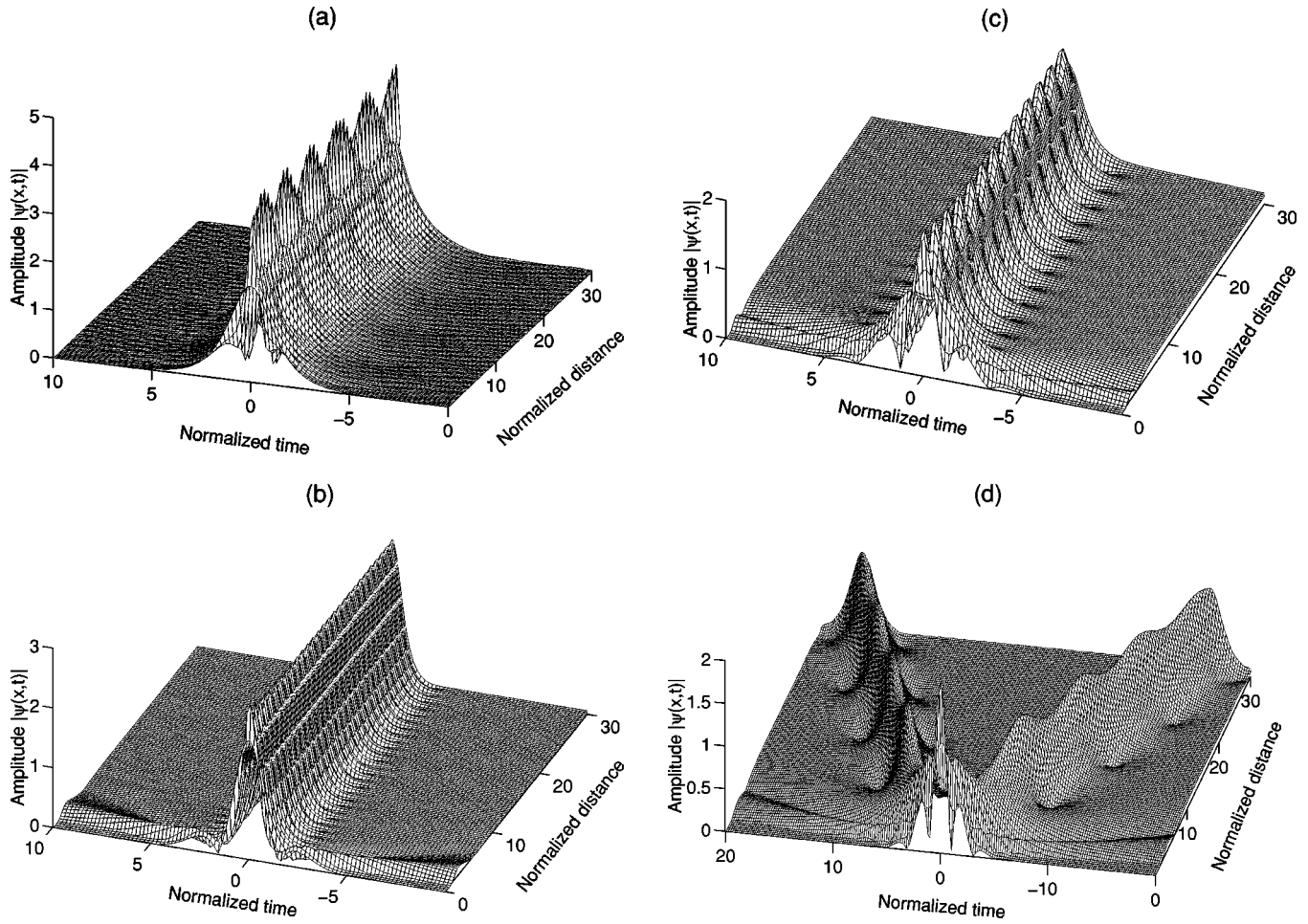

FIG. 2. The amplitude $|\psi(x,t)|$ versus the normalized distance t and normalized time x for symmetric initial conditions (24). (a) $\omega=0.1$; (b) $\omega=1.0$; (c) $\omega=1.4$; (d) $\omega=1.525$.

IV. SOLITON GENERATION FROM ANTISYMMETRIC INPUT PULSES

By a similar analysis with the one in the preceding section, in what follows we describe the structure of the optical field generated by an antisymmetric superposition of two fundamental solitons with different frequencies

$$\psi(x,0)=i[\mathrm{sech}(x)e^{i\omega x}-\mathrm{sech}(x)e^{-i\omega x}]. \tag{36}$$

Here, the imaginary unit was introduced only to ensure that the initial condition $\psi(x,0)$ is a real function. As before, the symmetry property $\psi(x,0)=-\psi(-x,0)$ extends to the matrix $U(x;\lambda)$:

$$U(x;\lambda)=-\sigma_2\overline{U}(-x;-\overline{\lambda})\sigma_2. \tag{37}$$

This involution property implies that if $F(x;\lambda)$ is an eigenfunction of Eq. (2) corresponding to the eigenvalue λ, then $\sigma_2\overline{F}(-x;\lambda)$ is an eigenfunction corresponding to the eigenvalue $-\overline{\lambda}$. Therefore, again the eigenvalues of the system (2) appear in pairs located symmetrically with respect to the imaginary axis. The asymptotic dependence (7) implies that, for $\mathrm{Im}\,\lambda>0$, the Jost functions must satisfy

$$T_-^{(1)}(x;\lambda)=i\sigma_2\overline{T}_+^{(2)}(-x;-\overline{\lambda}), \tag{38}$$

$$T_-^{(2)}(x;-\lambda)=-i\sigma_2\overline{T}_+^{(1)}(-x;\overline{\lambda}). \tag{39}$$

These involution properties show that Eqs. (28) and (29) describe this case too, so that the zeros of the scattering coefficient $a(\lambda)$ are located either on the imaginary axis or they appear in pairs at $(\lambda,-\overline{\lambda})$.

In what follows, we describe the case in which $a(\lambda)$ has only a pair of zeros at $(\lambda_0,-\overline{\lambda_0})$ with $\lambda_0=\xi+i\eta$, ξ, $\eta>0$, and $b(\lambda)=0$ for any real λ. One can see that in this case Eq. (38) implies that

$$\overline{\gamma}_+\gamma_-=-1. \tag{40}$$

As before, this relation is satisfied at any time t, that is, the soliton solution preserves its symmetry upon propagation. Furthermore, if we choose the initial values of γ's such that

$$\gamma_+(0)=-\gamma_-(0)=1, \tag{41}$$

then the initial conditions corresponding to these scattering data are real.

By solving the GLM equation (13) which corresponds to these scattering data, one obtains the following two-soliton solution:

$$\psi(x,t) = -i\xi\eta e^{\phi(t)} \frac{e^{i\xi x}\cosh[\eta(x+2\xi t)+i\varphi] - e^{-i\xi x}\cosh[\eta(x-2\xi t)-i\varphi]}{\xi^2\cosh\eta(x+2\xi t)\cosh\eta(x-2\xi t)+\eta^2\cos\xi(x+2i\eta t)\cos\xi(x-2i\eta t)}. \tag{42}$$

Such solitons can be excited if one considers as the initial condition of the NLSE (1) pulses with appropriate symmetry. In order to illustrate this fact, we determined the spectrum of the eigenvalue problem (2) which corresponds to the choice (36). The structure of this spectrum, as well as the dependence of the energies $E_{\rm in}$ and $E_{\rm rad}$ on the frequency detuning ω, is presented in Figs. 3(a)–3(b). As Fig. 3(a) illustrates, for frequency detuning $\omega<\omega_1^a\simeq 0.369$ no soliton is generated, while for $\omega>\omega_1^a$ the emerging solution represents the superposition of two solitons that exhibit equal amplitudes and opposite velocities, that is, a two-soliton solution described by Eq. (42). Furthermore, one can observe that, unlike the symmetric case, for antisymmetric input pulses with $\omega\simeq\omega_1^a$ the emerging soliton has a finite velocity. This fact can be understood as follows: if both the velocity ξ and the amplitude η would vanish, then the coefficient $a(\lambda)$ would have a zero in the origin. However, as we will show in the next section, this would require the area of the input pulse to be an odd multiple of $\pi/2$, a condition which cannot be satisfied by an antisymmetric function. Finally, similar to the symmetric case, the energy in the radiative modes $E_{\rm rad}$ has a maximum at $\omega=\omega_1^a$.

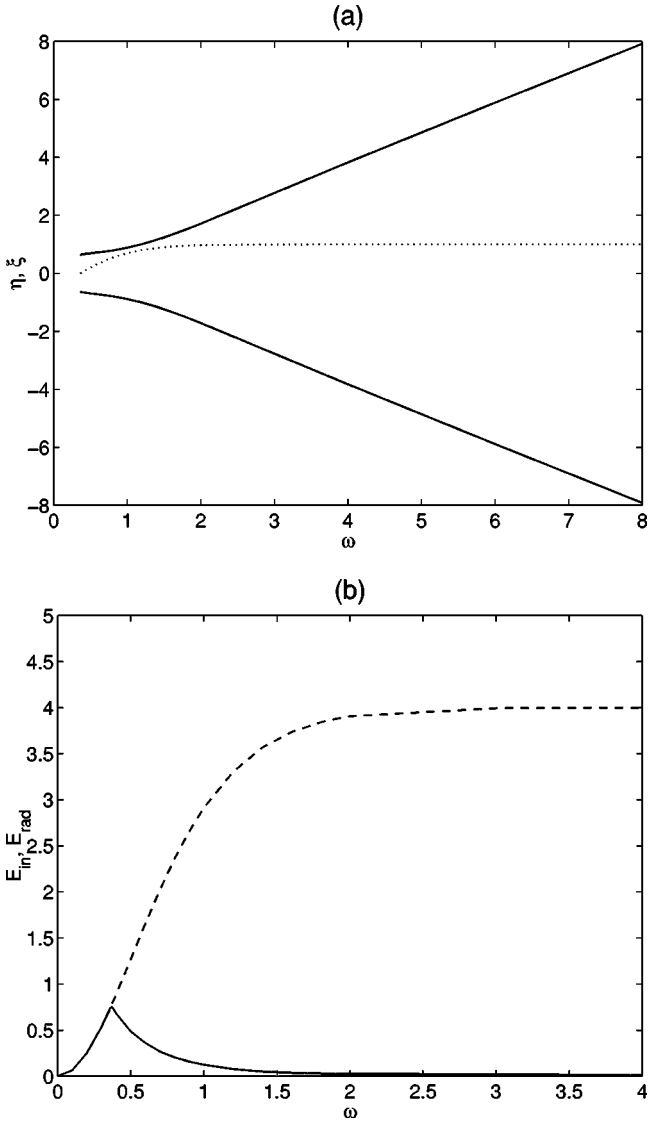

FIG. 3. The same as in Fig. 1, but for the antisymmetric input (36).

These results are also verified by the numerical simulation of the propagation of an input pulse (36) for various frequencies ω. Thus, as Figs. 4(a)–4(b) illustrate, for frequency $\omega=0.25<\omega_1^a$ no soliton is generated, while for $\omega=0.75>\omega_1^a$ the emerging solution represents the superposition of two solitons that exhibit equal amplitudes and opposite velocities.

V. THE NUMBER OF GENERATED SOLITONS

In what follows we will discuss the relationship between the structure of the spectra of the eigenvalue problem (2) and the initial area of the optical pulse. A similar discussion of

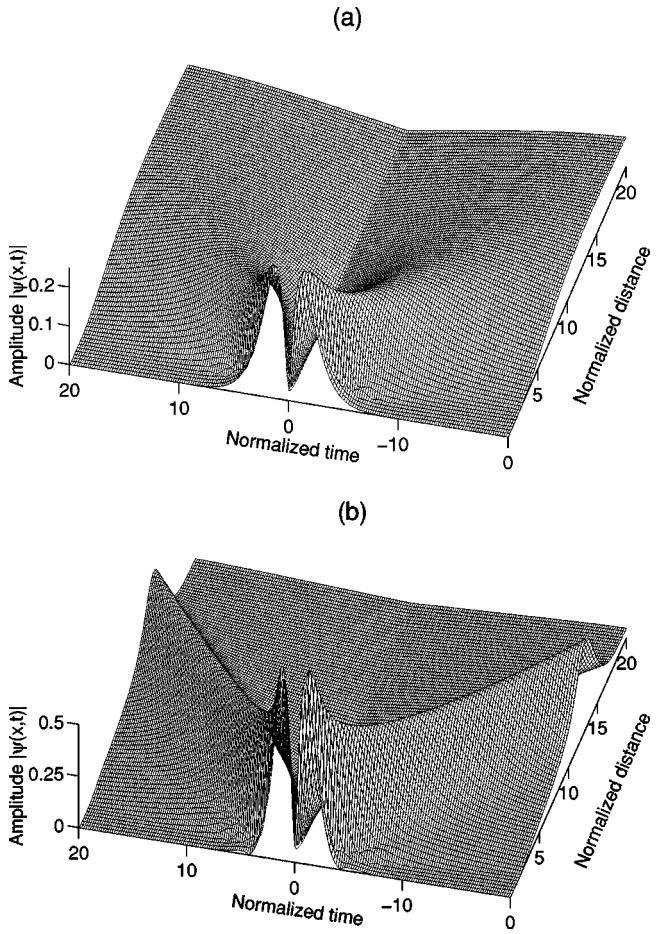

FIG. 4. The amplitude $|\psi(x,t)|$ versus the normalized distance t and normalized time x for antisymmetric initial conditions (36). (a) $\omega=0.25$; (b) $\omega=0.75$.

some of the results presented here can be found in [30–32]. To begin with, let us consider the system (2) for the particular value $\lambda=0$ and for real functions $\psi(x,0)$:

$$\frac{\partial F_1}{\partial x}=i\psi F_2, \tag{43}$$

$$\frac{\partial F_2}{\partial x}=i\psi F_1. \tag{44}$$

It is easy to see that the general solution of the system (43) and (44) can be written as

$$\begin{pmatrix} F_1 \\ F_2 \end{pmatrix}=\begin{pmatrix} e^{-iS(x)}\left(C_1\int_{-\infty}^{x}\psi(x',0)e^{2iS(x')}dx'+C_2\right) \\ -iC_1e^{iS(x)}-F_1 \end{pmatrix}, \tag{45}$$

where C_1, C_2 are arbitrary constants and

$$S(x)=\int_{-\infty}^{x}\psi(x',0)dx'. \tag{46}$$

Therefore, by taking into account the asymptotic conditions (7), one can see that the Jost function $T_{-}^{(1)}(x;0)$ is determined by the choice $C_1=i$, $C_2=1$. Furthermore, knowing the expression of the Jost function $T_{-}^{(1)}(x;0)$ and the asymptotic dependence $T_{+}^{(2)}(x;0)\rightarrow\binom{0}{1}$, $x\rightarrow\infty$, one can determine from Eq. (10) the scattering coefficient $a(0)$,

$$a(0)=e^{-iS_0}\left(i\int_{-\infty}^{\infty}\psi(x',0)e^{2iS(x')}dx'+1\right), \tag{47}$$

where $S_0=S(\infty)$ is the initial area of the pulse. A simple integration by parts in Eq. (47) leads to the final expression for $a(0)$:

$$a(0)=\cos S_0. \tag{48}$$

This formula has been used to predict the number of solitons which are generated from an optical pulse with a certain initial area. Thus, assuming that only solitons with zero velocities are generated and that, up to a constant phase, the initial condition $\psi(x,0)$ is real, it was argued that the number N of solitons is given by [31,32]

$$N=\left[\frac{1}{2}+\frac{S_0}{\pi}\right], \tag{49}$$

where [ ] is the largest integer smaller than the argument. However, a more rigorous restatement of Eq. (49) is that in order to generate a soliton with zero amplitude and velocity, that is, $a(0)=0$, the area S_0 of the initial pulse must satisfy

$$S_0=(2n-1)\frac{\pi}{2}, \tag{50}$$

where n is an arbitrary integer. When applied to the symmetric case, Eq. (50) has the following solutions: $\tilde{\omega}_1=0.506$ for $n=2$ and $\tilde{\omega}_2=1.313$ for $n=1$. We see that these values are in excellent agreement with the threshold frequencies $\omega_{1,2}^{s}$. The fact that Eq. (49) can lead to wrong results is illustrated by the discrete spectrum shown in Fig. 1(a). Thus, for $\omega_2^s<\omega<\omega_3^s$, Eq. (49) predicts that no soliton with zero velocity can be generated, a conclusion which is obviously wrong.

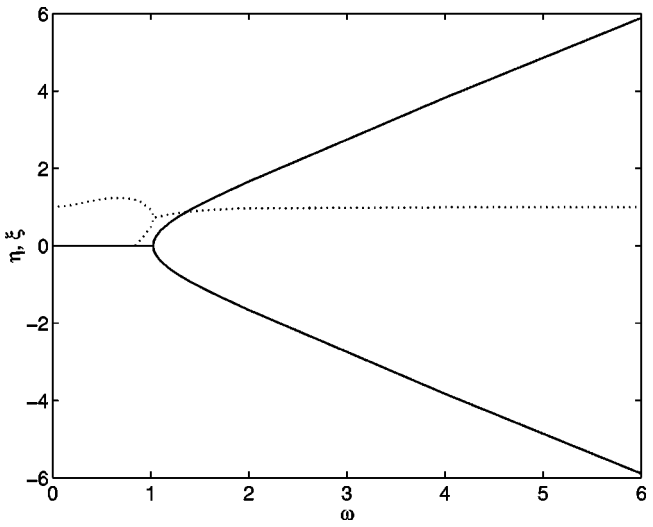

FIG. 5. The discrete spectrum determined by the initial condition (51). The amplitude η (dotted line) and the velocity ξ (continuous line) of the generated solitons as a function of the frequency detuning ω. The phase difference is $\theta=2\pi/3$.

To conclude this section, we will illustrate how Eq. (50) can be used to describe the structure of the eigenvalue spectrum associated with the following initial condition:

$$\psi(x,0)=\mathrm{sech}(x)e^{i[\omega x+(\theta/2)]}+\mathrm{sech}(x)e^{-i[\omega x+(\theta/2)]}. \tag{51}$$

This expression represents the superposition of two fundamental solitons with different frequencies and phases. The phase difference between the two solitons is θ. The symmetric and antisymmetric initial conditions can be obtained from Eq. (51) by choosing $\theta=0$ and $\theta=\pi$, respectively.

The initial area of the optical pulse described by Eq. (51) is

$$S_0(\omega,\theta)=2\pi\,\mathrm{sech}\left(\frac{\pi\omega}{2}\right)\cos\left(\frac{\theta}{2}\right). \tag{52}$$

From Eqs. (50) and (52) one can see that if $\omega=0$, there are two critical values of the phase difference θ for which $a(0)=0$. The two critical values are $\theta_{\mathrm{cr}}^{(1)}=2\arccos(\frac{3}{4})$ and $\theta_{\mathrm{cr}}^{(2)}=2\arccos(\frac{1}{4})$ and correspond to $n=2$ and $n=1$, respectively. This implies that at $\omega=0$, depending on the value of the phase difference θ, there are two distinct eigenvalues located on the imaginary axis if $0\leqslant\theta<\theta_{\mathrm{cr}}^{(1)}$, one if $\theta_{\mathrm{cr}}^{(1)}<\theta<\theta_{\mathrm{cr}}^{(2)}$, and none if $\theta_{\mathrm{cr}}^{(2)}<\theta\leqslant\pi$. Consequently, the eigenvalue spectra in the first and the third case are topologically similar to the ones presented in Fig. 1(a) and Fig. 3(a), respectively. A typical spectrum which corresponds to the second case, that is, $\theta_{\mathrm{cr}}^{(1)}<\theta<\theta_{\mathrm{cr}}^{(2)}$, is presented in Fig. 5 and is obtained for $\theta=2\pi/3$.

VI. CONCLUSIONS

In conclusion, we have described the interaction between two overlapping solitons of different frequencies which propagate in an ideal monomode optical fiber. We analyzed the physical regime in which the frequency detuning is comparable to the soliton spectral width. It has been shown that, depending on the separation in the initial frequencies, the structure of the generated solitons can be very rich. Thus, it is possible to generate one or two solitons with zero velocities in the group velocity reference frame or a pair of solitons which propagate with equal and opposite velocities. The thresholds which separate these different regimes are calculated both analytically and numerically. Finally, we would like to stress that in order to generate solitons of the type (32) and (42), the choice of the initial pulses is not restricted to sech-like type. Thus, we determined the structure of the emerging solitons from a superposition of two Gaussian pulses and the results we obtained were qualitatively similar to those presented here, the only difference consisting in the numerical values of the threshold frequencies $\omega^s_{1,2,3}, \omega^a_1$. Therefore, the results we presented are rather general and not restricted to a specific form of the two superimposed pulses.

ACKNOWLEDGMENTS

This work was supported in part by the Russian Foundation for Basic Research and by the Russian Ministry for Science and Technology program ''Nanostructures.'' C.E. and F.L. thank the Deutsche Forschungsgemeinshaft (INK1) for support. We gratefully thank M.J. Ablowitz, G. Biondini, J. Cole, J.W. Haus, R.L. Horne, and K. Wagner for many helpful discussions.

[1] A. Hasegawa and F. Tappert, Appl. Phys. Lett. **23**, 142 (1973); **23**, 171 (1973).
[2] V. E. Zakharov and A. B. Shabat, Zh. Éksp. Teor. Fiz. **61**, 118 (1971) [Sov. Phys. JETP **34**, 62 (1972)]; **64**, 1627 (1973) [**37**, 823 (1973)].
[3] L. F. Mollenauer, R. H. Stolen, and J. P. Gordon, Phys. Rev. Lett. **45**, 1095 (1980).
[4] P. Emplit, J. P. Hamaide, F. Reynaud, G. Froehly, and A. Barthelemy, Opt. Commun. **62**, 374 (1987); D. Krökel, N. J. Halas, G. Giuliani, and D. Grischkowski, Phys. Rev. Lett. **60**, 29 (1988); A. M. Weiner, J. P. Heritage, R. J. Hawkins, R. N. Thurston, E. M. Kirschner, D. E. Leaird, and W. J. Tomlinson, *ibid.* **61**, 2445 (1988).
[5] J. Satsuma and N. Yajima, Prog. Theor. Phys. Suppl. **55**, 284 (1974).
[6] V. I. Karpman and V. V. Solov'ev, Physica D **3**, 487 (1981).
[7] Y. Kodama and A. Hasegawa, Opt. Lett. **16**, 208 (1991).
[8] A. Hasegawa and Y. Kodama, *Solitons in Optical Communications* (Oxford University Press, Oxford, 1995).
[9] V. S. Gerdjikov, D. J. Kaup, I. M. Uzunov, and E. G. Evstatiev, Phys. Rev. Lett. **77**, 3943 (1996); V. S. Gerdjikov, I. M. Uzunov, E. G. Evstatiev, and G. L. Diankov, Phys. Rev. E **55**, 6039 (1997).
[10] C. Desem and P. L. Chu, in *Optical Solitons—Theory and Experiment*, edited by J. R. Taylor (Cambridge University Press, Cambridge, England, 1992), p. 127.
[11] Y. Kodama and K. Nozaki, Opt. Lett. **12**, 1038 (1987).
[12] T. Yamada and K. Nozaki, J. Phys. Soc. Jpn. **58**, 1944 (1989).
[13] V. V. Afanasjev, V. A. Vysloukh, and V. N. Serkin, Opt. Lett. **15**, 489 (1990).
[14] Y. Kodama, M. Romagnoli, and S. Wabnitz, Electron. Lett. **28**, 1981 (1992).
[15] T. Georges and F. Favre, J. Opt. Soc. Am. B **10**, 1880 (1993).
[16] V. V. Afanasjev, Opt. Lett. **18**, 790 (1993).
[17] Y. Kodama and S. Wabnitz, Opt. Lett. **18**, 1311 (1993); **19**, 162 (1994).
[18] A. B. Aceves, C. D. Angelis, G. Nalesso, and M. Santagiustina, Opt. Lett. **19**, 2104 (1994).
[19] T. Okamawari, A. Hasegawa, and Y. Kodama, Phys. Rev. A **51**, 3203 (1995).
[20] I. M. Uzunov, M. Gölles, L. Leine, and F. Lederer, Opt. Commun. **110**, 465 (1994); I. M. Uzunov, M. Gölles, and F. Lederer, Phys. Rev. E **52**, 1059 (1995); J. Opt. Soc. Am. B **12**, 1164 (1995).
[21] P. A. Andrekson, N. A. Olsson, J. R. Simpson, T. Tanbun-Ek, R. A. Logan, P. C. Becker, and K. W. Wecht, Appl. Phys. Lett. **57**, 1715 (1990); P. A. Andrekson, N. A. Olsson, J. R. Simpson, T. Tanbun-Ek, R. A. Logan, and K. W. Wecht, Electron. Lett. **26**, 1499 (1990); **27**, 695 (1991).
[22] T. Aakjer, J. H. Povlsen, and K. Rottwitt, Opt. Lett. **18**, 1908 (1993).
[23] P. V. Mamyshev and L. F. Mollenauer, Opt. Lett. **21**, 396 (1996).
[24] M. J. Ablowitz, G. Biondini, S. Chakravarty, R. B. Jenkins, and J. R. Sauer, Opt. Lett. **21**, 1646 (1996).
[25] L. D. Faddeev and L. A. Takhtajan, *Hamiltonian Methods in the Theory of Solitons* (Springer-Verlag, New York, 1987).
[26] N. Sasa and J. Satsuma, J. Phys. Soc. Jpn. **60**, 409 (1991).
[27] D. Mihalache, L. Torner, F. Moldoveanu, N. C. Panoiu, and N. Truta, J. Phys. A **26**, L757 (1993); Phys. Rev. E **48**, 4699 (1993); D. Mihalache, N. C. Panoiu, F. Moldoveanu, and D. M. Baboiu, J. Phys. A **27**, 6177 (1994).
[28] D. Mihalache, N. C. Panoiu, F. Moldoveanu, D. Mazilu, and D. M. Baboiu, Proc. SPIE **2461**, 226 (1995).
[29] G. Boffetta and A. R. Osborne, J. Comput. Phys. **102**, 252 (1992).
[30] A. B. Shvartsburg and M. A. Zuev, Opt. Quantum Electron. **12**, 95 (1980).
[31] J. Burzlaff, J. Phys. A **21**, 561 (1988).
[32] Y. S. Kivshar, J. Phys. A **22**, 337 (1989).